Experimental observation of a strong mean flow induced by internal gravity waves

Guilhem Bordes, Antoine Venaille, Sylvain Joubaud, Philippe Odier, Thierry Dauxois

Experimental observation of a strong mean flow induced by internal gravity waves

Guilhem Bordes,[1, a)] Antoine Venaille,[1, b)] Sylvain Joubaud,[1, c)] Philippe Odier,[1, d)] and Thierry Dauxois[1, e)]

[1] *Laboratoire de Physique de l'École Normale Supérieure de Lyon, CNRS and Université de Lyon, 46 Allée d'Italie, 69007 Lyon, France*

(Dated: 13 March 2012)

We report the experimental observation of a robust horizontal mean flow induced by internal gravity waves. A wave beam is forced at the lateral boundary of a tank filled with a linearly stratified fluid initially at rest. After a transient regime, a strong jet appears in the wave beam, with horizontal recirculations outside the wave beam. We present a simple physical mechanism predicting the growth rate of the mean flow and its initial spatial structure. We find good agreement with experimental results.

[a)] Electronic mail: guilhem.bordes@ens-lyon.fr
[b)] Electronic mail: antoine.venaille@ens-lyon.fr
[c)] Electronic mail: sylvain.joubaud@ens-lyon.fr
[d)] Electronic mail: philippe.odier@ens-lyon.fr
[e)] Electronic mail: thierry.dauxois@ens-lyon.fr

Introduction. Stratified fluids support the existence of anisotropic dispersive waves, called internal gravity waves, which play a major role in astrophysical and geophysical fluid dynamics[1,2]. Recent technical advances allowing for accurate visualization[3,4] and well controlled wave generation[5,6] in laboratory experiments have provided a renewal of interest in this field[7]. Previous laboratory experiments focused mostly on propagative wave beams in narrow tanks[5,6,8] or propagative vertical modes[9,10]. Here we consider the case of a propagative wave beam in a wide tank, which remains largely unexplored, despite its physical importance.

A central aspect of wave dynamics is the possible generation of a mean flow due to nonlinearities involving one or several wave beams. These phenomena have important consequences for geophysical flow modeling, since they imply backward energy transfers, or large scale transport properties induced by small scale motions. Among all waves, internal waves are very peculiar because of the specific and unusual nature of nonlinearity. For instance, it has been reported[12,13] that in some important cases, the leading nonlinear term unexpectedly cancels out if one has just one internal wave beam.

King, Zhang and Swinney[15] have recently reported the generation of a mean flow by nonlinearities in the presence of internal gravity waves. However, the structure of the observed mean flow has not been explained, and the underlying mechanism of generation has not yet been proposed. Here we propose a physical mechanism for such a phenomenon, supported by strong experimental evidences. There have been numerous theoretical studies of internal gravity waves-mean flow interactions, see e.g. Refs.[13,16,17], but none of them considered the case of propagative waves with a slowly varying amplitude in three dimensions. We will show that in our experiments, both viscous attenuation and lateral variations of the wave beam amplitude play a key role in the generation of the observed mean flow.

The paper is organized as follows. We first present the experimental setup. Then we provide detailed observations of the wave field and of the mean flow. We finally propose a mechanism to deduce the spatial structure of the mean flow and the temporal evolution of its amplitude from the measurements of the wave field.

Experimental setup. We consider a 120 cm long, 80 cm wide and 42.5 cm deep wave tank, filled with 35 cm of salt water, see Fig. 1(a). The fluid is linearly stratified in density with a Brunt-Väisälä frequency $N = \sqrt{-(g/\rho)\partial_z \rho}$, where g is the local gravity, ρ the density of the fluid and z the vertical coordinate. An internal wave generator is placed on one side of the tank, see Refs.[5,6] for its full presentation and characterization; it is made of a series of 18 rectangular plates stacked around a helical camshaft. The plates, which are 14 cm wide in the y-direction, oscillate back and forth along the longitudinal horizontal coordinate x. The phase shifts between successive cams are chosen in order to form a sinusoidal profile at the surface of the generator. The rotation of the camshaft at a frequency $\omega \leq N$ generates a moving boundary condition with an upward or downward phase velocity depending on the sign of the rotation of the helical camshaft. The displacement profile is $X_0(t, z) = x_0 \sin(\omega t - mz)$, with a vertical wavelength $\lambda_z = 2\pi/m = 3.8$ cm and an amplitude $x_0 = 0.5$ cm or $x_0 = 1$ cm.

In the experiments, the front face of the wave generator is located at $x = 0$, centered at $y = 0, z = 15.8$ cm. The wave beam is 14 cm wide, 11.4 cm high, corresponding to three wavelengths. The generator is only forcing the x-component of the internal wave, while the z component is found to adjust according to the internal wave structure. The propagation angle θ of the internal wave is varied by changing the rotation rate of the wavemaker motor, while keeping the Brunt-Väisälä frequency constant between each experiment, namely $N = 0.85$ rad s^{-1}. Importantly, this experimental set-up leads to a wave amplitude that depends on the frequency[6]. Moreover, the axis of the wavemaker camshaft staying always vertical, the efficiency of the forcing depends significantly on the projection of the plate motion on the direction of propagation. The wavemaker frequency being varied in the range $\omega = 0.26\,N$ to $0.50\,N$, corresponding to an angle of propagation θ from 15° to 30°, the amplitude of the wave is measured experimentally.

Velocity fields are obtained using a 2D particle image velocimetry (PIV) system[3,18]. The flow is seeded with 10 μm tracer particles, and illuminated by a 532 nm 2W-continuous laser, shaped into a vertical or horizontal sheet. Respectively, a vertical 35×43 cm^2 or horizontal 33×43 cm^2 field of view is acquired by a 8-bit 1024×1024 pixels camera. For each wavemaker frequency, a set of 600 to 1600 images is recorded, at a frequency of 0.38 to 1.25 Hz, representing 10 images per wavemaker period. PIV computations are performed over successive images, on 21×21 pixels interrogation windows with 50% overlap. The spatial resolution is approximately 25×25 px/cm^2. A snapshot of the particle flow is presented in Fig. 1(b).

Experimental results. We denote $\mathbf{u} = (u, v, w) = \mathbf{u'} + \mathbf{u_0}$ the velocity field in Cartesian coordinates $\mathbf{x} = (x, y, z)$, with $\mathbf{u'}$ the "wave" part oscillating at a frequency ω set by the

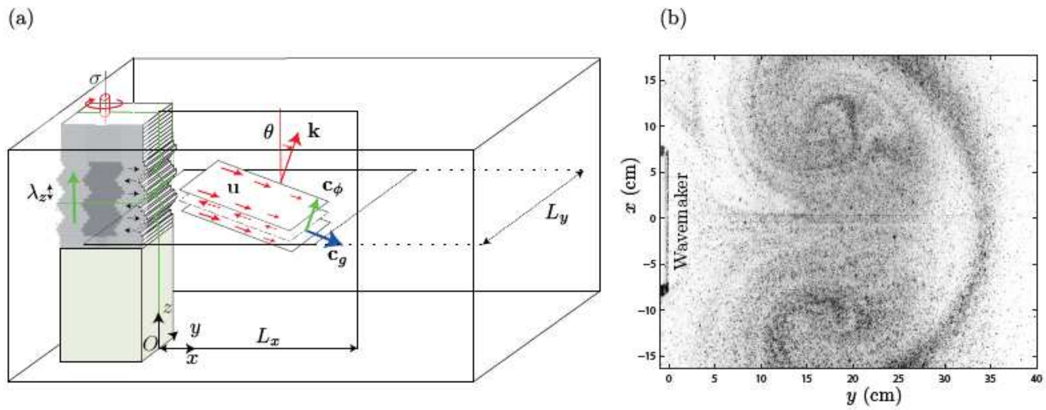

FIG. 1. (Color online) (a) Schematic representation of the experimental set-up. The wave generator is placed on one side of the tank, defining the origin of the spatial coordinates. The excited plane internal wave has a frequency ω, an upward phase velocity and propagates with an angle $\theta = \sin^{-1}(\omega/N)$. (b) Top view of the particle flow in the horizontal plane $z = 21.6$ cm.

wave generator and $\mathbf{u_0}$ the dc-component of the velocity field. The latter corresponds to a large scale structure of the flow, which will be referred to as "mean flow" in the following (see Fig. 1(b)).

Selective Fourier filtering of the measured horizontal velocity field allows to extract the spatial structure of the wave from the mean flow. The wave horizontal velocity field is obtained using a bandpass filter centered on ω, with a width of $0.014\,\omega$ and is presented in Fig. 2(a) and (b). Figure 2(a) shows a vertical slice taken at the center of the generator ($y = 0$). We notice the three wavelengths, the amplitude decay in the x-direction, and the approximately constant amplitude along the z-direction. Figure 2(b) presents a horizontal slice located around the mid-depth of the generator showing the wave amplitude variations in the y-direction.

The above experimental observations readily suggest to assume that the imposed wave $(u', 0, w')$ is monochromatic, with an amplitude varying in space, and that it can be expressed in terms of a stream function as follows

$$\psi = \Psi(x, y, z) \cos(\omega t - kx - mz), \quad u' = -\partial_z \psi, \quad w' = \partial_x \psi \ , \tag{1}$$

since the horizontal transversal component v' is vanishingly small and will be neglected in what follows. The experimental observations also strongly suggest that the variations of $\Psi(x, y, z)$ appears on a much larger length scale than the wavelength of the internal wave

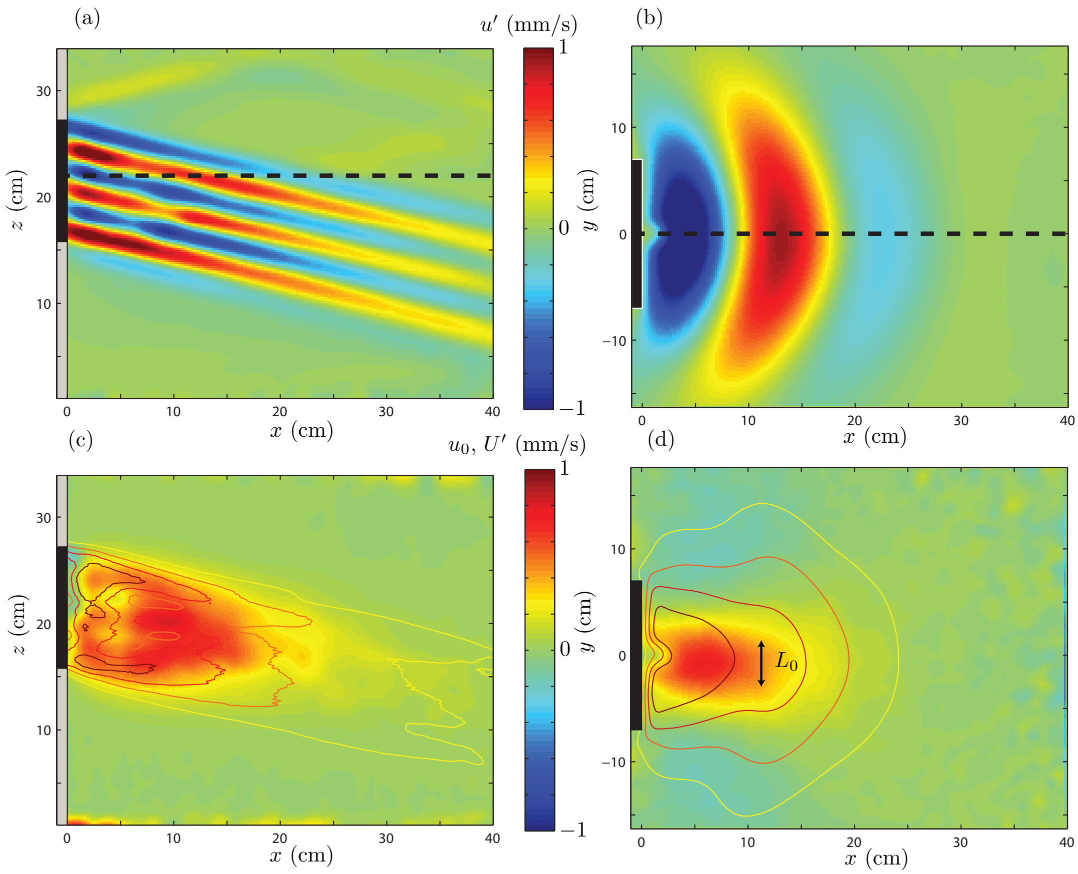

FIG. 2. (Color online) (a) and (b): Experimental wave field, u', obtained by filtering the horizontal velocity field at ω. (c) and (d): Experimental mean flow, u_0, obtained by low-pass filtering the horizontal velocity field. The contours represent the amplitude of the wave horizontal velocity field, U'. The left panels (a) and (c) present the side view and the right panels (b) and (d) present the top view. All pictures were obtained for $\omega/N = 0.26$ and a 1 cm eccentricity for the cams. The wavemaker is represented in grey and the moving plates in black. The dashed line in (a) (respectively (b)) indicates the field of view of (b) (respectively (a)).

beam.

Let us now consider the low-pass filtered flow, which we call "mean flow". The width of the filter used to extract the mean flow is $0.25\,\omega$. A strong jet going in the outward direction from the generator is observed in Fig. 2(c) and (d). This structure is initially located close to the generator, then grows until it fills the whole plane. We observe that the jet is precisely produced inside the wave beam. Recirculations on the sides of the tank are visible in Fig. 1(b) and in Fig. 2(d) through the blue patches. These recirculations clearly show that the horizontal mean flow is characterized by non-zero vertical vorticity.

Introducing L the length of the tank and U the characteristic scale of the velocity field, the horizontal fluid motions $(u_0, v_0, 0)$ are characterized by an eddy turnover time $T_{mean} = L/U$. A key assumption at this stage is to consider that the eddy turnover time is large with respect to the wave period, the timescale of the internal wave. This regime, $T_{mean} \gg 2\pi/\omega$ corresponds to a low Froude number limit $U/(NL) \ll 1$ in which vertical motions are inhibited, allowing to neglect the vertical velocity: $w_0 \ll w'$, which is supported by experimental observations.

Interpretation. Using the ansatz (1) motivated by experimental results, it is possible to go further and propose a modelisation which captures the essence of the physical mechanism underlying the generation of a strong mean flow by the internal wave beam. Considering a fluid in the Boussinesq approximation[2], the dynamics of the vertical component of the vorticity $\mathbf{\Omega} = \nabla \times \mathbf{u}$ is given by

$$\partial_t \Omega_z + \mathbf{u} \cdot \nabla \Omega_z = \mathbf{\Omega} \cdot \nabla w + \nu \Delta \Omega_z \ . \tag{2}$$

Averaging over a wave period, T_{wave}, with the operator $\overline{A} = (1/T_{wave}) \int_t^{t+T_{wave}} \mathrm{d}t' \ A(t')$, and assuming that horizontal motions do not depend on the fast time scale so that one has $(\overline{u_0}, \overline{v_0}) \approx (u_0, v_0)$, yields

$$\partial_t \Omega_{0z} + \mathbf{u}_0 \cdot \nabla \Omega_{0z} = \partial_y \left[\overline{\partial_x u'^2} + \overline{\partial_z (w'u')} \right] + \nu \Delta \Omega_{0z} \ , \tag{3}$$

where we introduced $\Omega_{0z} = \partial_x v_0 - \partial_y u_0$, the vertical component of the vorticity of the mean flow. Nonlinear terms act therefore as a source of vertical vorticity, through the lateral variations (in the y-direction) of the divergence of the quantity $\overline{u'u'}\mathbf{e}_x + \overline{w'u'}\mathbf{e}_z$, in the same manner as the Reynolds stress tensor in a turbulent flow acts as a source of turbulent transport.

Using the ansatz (1), the nonlinear term of Eq. (3) can be explicitly computed, which yields

$$\partial_t \Omega_{0z} + \mathbf{u}_0 \cdot \nabla \Omega_{0z} = \frac{1}{2} \partial_y \left[m^2 \partial_x (\Psi^2) - km \partial_z (\Psi^2) \right] + \nu \Delta \Omega_{0z} \ , \tag{4}$$

where it has been assumed that the wavelength is much smaller than typical spatial variations of the wave amplitude. This scale separation is satisfied in the bulk of the wave region, but not in its edges. However, this technical hypothesis allows a simple physical understanding of the dynamics, fully sufficient here.

A first consequence of Eq. (4) is that nonlinearities cannot be a source of vertical vorticity Ω_{0z} if the wave field is invariant in the y-direction. In our experiments, the wave generator occupies only one part of the tank width, so one might expect horizontal variations of the wave amplitude, which fulfills the necessary condition to observe generation of a horizontal mean flow associated with non-zero vertical vorticity. A second consequence is that if the wave field is symmetric in the y-direction then the source term in Eq. (4), resulting from a derivation of the wave field with respect to y, is antisymmetric in the y-direction. This is the case in our experiments, because the wavemaker is symmetric with respect to y. A third consequence is that variations in the x or z directions are necessary to produce vertical vorticity. Such variations can be due to viscosity, in which case the wave amplitude decays away from the generator[1,19] with a typical lengthscale defined as ℓ. Reference[13] reported that a single wave beam could not generate a mean flow in a two-dimensional (or axi-symmetric) configuration, with invariance in the y-direction. This is consistent with our finding that the generation of a mean flow requires variations of the wave-amplitude in the y direction. Refs.[13,14] also showed that a mean flow can be generated by two interacting wave beams, even if there is no variation of the wave amplitude in the y direction. Again, there is no contradiction with our results, because the mean flow they describe is associated with zero vertical vorticity, due to their invariance in the y direction.

Finally, let us describe the spatial structure of the nonlinear term of Eq. (4) in our experimental setup. It is a reasonable approximation to assume $\partial_z (\Psi^2) \approx 0$ at mid-depth of the wave field (see Fig. 2(a)) and $\Psi(x, y) = \Pi(y)e^{-x/\ell}$. The typical length scale of viscous attenuation ℓ can be estimated[19] around 20 cm, which means that viscosity will play an important role in this experiment. The generator induces a symmetric wave field in the y-direction, maximum at the origin, satisfying $\partial_y (m^2\partial_x\Psi^2) > 0$ for $y > 0$ and $\partial_y (m^2\partial_x\Psi^2) < 0$ for $y < 0$. According to Eq. (4), we conclude that the source term induces a dipolar vorticity structure associated with a horizontal jet going in the outward direction from the wave generator.

For the sake of simplicity, we have assumed in this paper that the wave field is given, and we have neglected any feedbacks due to the formation of the mean horizontal flow. Future work will include a more complete and more rigorous analytical treatment of this problem, with the appropriate multiscales development.

The horizontal slice shown in Fig. 2(d) is centered on the middle plate of the wavemaker (dashed line in Fig. 2(a)), so we can assume $\partial_z\Psi^2=0$ in Eq. (4), except at the top and bottom edges of the wave beam (see Fig. 2(a)). Assuming also that the wave beam is sufficiently damped by viscosity as its top edge crosses the horizontal slice, we will neglect the term $\partial_z\Psi^2$ everywhere.

Assuming finally that the wavelength $2\pi/m$ is much smaller than typical spatial variations of Ψ^2, the wave stream function is given by $\Psi = U'/m$, where U' is the amplitude of the horizontal velocity field of the wave, $u' = -U'(x,y,z)\sin(\omega t - kx - mz)$. Equation (4) becomes

$$\partial_t\Omega_{0z} + \mathbf{u}_0\cdot\nabla\Omega_{0z} = \frac{1}{2}\partial_{xy}U'^2 \; + \nu\Delta\Omega_{0z}. \tag{5}$$

For sufficiently short times, the nonlinear term and the viscous term can be neglected, and one expects that $\partial_t\Omega_{0z} \simeq \partial_{xy}U'^2/2$. The experimental determinations of these two terms are compared in Fig. 3 for $t = 106$ s. This time is much smaller than the viscous time (~ 1000 s) described in the last part of this paper. The magnitude of $\partial_t\Omega_{0z}$ (Fig. 3(a)) is of the order of the source term (Fig. 3(b)) and both fields correspond well spatially. The inset in Figure 3(a) shows a good spatial correlation between both fields. The slope that relates the two terms is 0.46 ($\pm$0.04), although the theory predicts 1. This difference may be due to contributions of the vertical variations of the wave amplitude in the experiments.

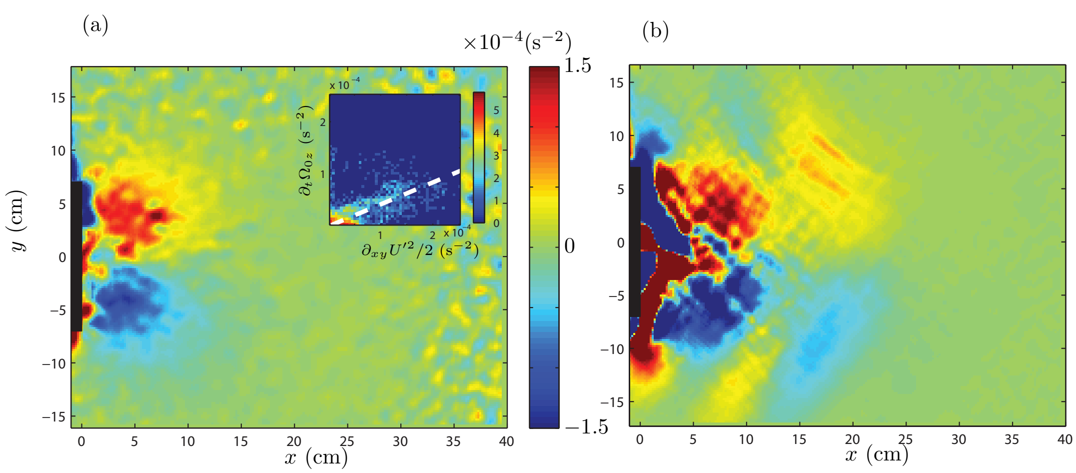

FIG. 3. Panels (a) and (b) present the top view in the $z = 21.6$ cm plane at $t = 106$ s of the two important quantities entering in Eq. (5): $\partial_t\Omega_{0z}$ in the left panel and $\partial_{xy}U'^2/2$ in the right panel. Both pictures were obtained for $\omega/N = 0.26$ and a 1 cm eccentricity for the cams. The inset in the left panel presents the 2D-histogram of $\partial_t\Omega_{0z}$ versus $\partial_{xy}U'^2/2$ to emphasize the correlation between both quantities. The dotted line corresponds to the slope 0.46 ($\pm$0.04) discussed in the text.

In order to address the temporal evolution of the mean horizontal flow at mid-depth of the wavemaker, it is convenient to integrate Eq. (5) over a domain defined as a half-plane of Fig. 3(b) (domain $\mathcal{D}^+ = [0, L_x] \times [0,\ L_y/2]$). This procedure cancels exactly the nonlinear term, even if it may be locally important. Indeed, using $\mathbf{u}_0 \cdot \nabla \Omega_{0z} = \nabla \cdot (\Omega_{0z} \mathbf{u}_0)$, the surface integral of this term vanishes since Ω_{0z} is zero on the Ox axis and the velocity $\mathbf{u}_0$ is zero on the other edges of the domain. One obtains

$$\partial_t \iint_{\mathcal{D}^+} \mathrm{d}x \mathrm{d}y \, \Omega_{0z} = \frac{U'^2(0,0,z)}{2} + \nu \iint_{\mathcal{D}^+} \mathrm{d}x \mathrm{d}y \ \Delta \Omega_{0z}. \tag{6}$$

The integral in the left-hand side of this equation, which we call $I(z,t)$, can be transformed as (if we denote $\mathcal{C}^+$ the circulation path surrounding the domain $\mathcal{D}^+$)

$$I(z,t) \equiv \iint_{\mathcal{D}^+} \mathrm{d}x \mathrm{d}y \ \Omega_{0z}(x,y,z,t) = \oint_{\mathcal{C}^+} \mathrm{d}\mathbf{l} \cdot \mathbf{u}_0 \approx \int_0^{L_x} \mathrm{d}x \ \mathbf{u}_0, \tag{7}$$

since along $\mathcal{C}^+$, the velocity is non zero only on the y=0 axis. In this form, $I(z,t)$ can be identified as a measure of the jet strength. Equation (6) can then be written as

$$\partial_t I(z,t) = \frac{U'^2(0,0,z)}{2} + \nu \iint_{\mathcal{D}^+} \mathrm{d}x \mathrm{d}y \ \Delta \Omega_{0z}. \tag{8}$$

Finally, defining L_0 as the smallest characteristic scale, ie along y, of the vorticity Ω_{0z}, the viscous term may be approximated by $-\nu I(z,t)/L_0^2$. The jet strength is then solution of a first order differential equation,

$$\partial_t I(z,t) = S - \frac{\nu}{L_0^2} I(z,t), \tag{9}$$

where S is the source term $S = U'^2(0,0,z)/2$. Equation (9) shows that the jet strength $I(z,t)$ should vary exponentially with time and one gets

$$I(z,t) = \frac{S L_0^2}{\nu} \left(1 - e^{-\nu t / L_0^2} \right) . \tag{10}$$

We observe such an exponential growth in Fig. 4(a), which represents the time evolution of the quantity $I(z,t)$ for different values of S and $z = 21.6$ cm. A deviation from the exponential growth happens at large times when the mean flow reaches the side of the visualization window, in which case the integral $I(z,t)$ saturates since the approximation of Eq. 7 is not valid any more. The value of L_0^2 is estimated by an exponential fit of the evolution of $I(z,t)$ as a function of time. Remarkably, one gets the same characteristic scale

$L_0 \approx 4$ cm for all experiments, which corresponds to the jet width shown in Fig. 2(d). We then estimate experimentally the source term in two different ways: the exponential fit (S_{fit}) and the measurement of the amplitude of the horizontal velocity field ($S_{\text{exp}} = U'(0,0,z)^2/2$). S_{fit} is plotted as a function of S_{exp} in Fig. 4(b). As expected, a linear relation between these two estimations is obtained. We find $S_{\text{fit}} = (0.45 \pm 0.02)\, S_{\text{exp}}$ in agreement with the spatial correlation observed in the inset of Fig. 3(a). However our simple model predicts $S_{\text{fit}} = S_{\text{exp}}$. This shows that the present theoretical explanation is valid qualitatively but is not fully sufficient to estimate quantitatively the strength of the jet.

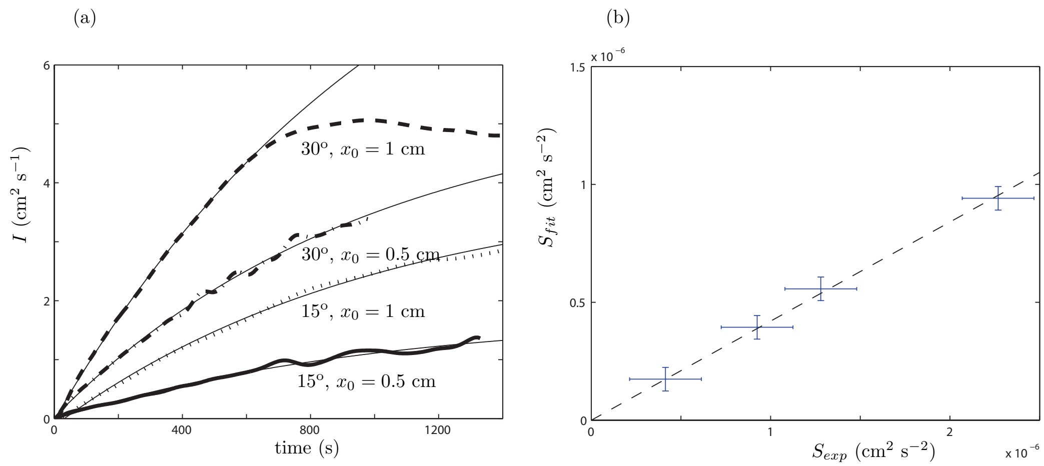

FIG. 4. Panel (a) presents the evolution vs time of the quantity $I(z_0, t)$, with exponential fits. Panel (b) shows the value S_{fit} of the source term estimated from the exponential fits of panel (a) vs the experimental estimation S_{exp} of the same source term. The dashed line corresponds to $S_{\text{fit}} = (0.45 \pm 0.02)\, S_{\text{exp}}$.

Conclusion. We have reported experimental observations of a strong horizontal mean flow with non-zero vertical vorticity when a propagative monochromatic wave is forced on the side of a tank filled with a linearly stratified fluid. We stress here that there is no such mean flow in absence of internal waves propagation, for example when the generator is excited at a frequency ω larger than the Brunt-Väisälä frequency N, as in Ref.[15].

The key ingredient for the existence of this mean vertical vorticity with a dipolar structure, associated with a strong horizontal jet flowing outward of the generator is the concomitant existence of variations of the wave amplitude in both horizontal directions. In the transverse direction (y), the variations are simply due to the fact that the wave generator is localized in a segment smaller than the tank width. In the longitudinal direction, the variations of the wave amplitude are due to viscous attenuation. This shows the important role played by viscosity in the generation of the mean flow in our experiments.

However, we believe that the mechanism given here for the generation of a strong mean flow by interactions between monochromatic waves has interest beyond the viscous regime: any physical process that leads to variations of the wave amplitude may lead to the formation of a robust horizontal mean flow. Such variations in the wave amplitude may be for instance due to parametric subharmonic instabilities[10], wave breaking[9], superposition of different wave beams[20] or generation of collimated internal tide beams[21]. This will be the object of future work.

ACKNOWLEDGMENTS

The authors thank M. Lasbleis for preliminary experiments. ENS Lyon's research work has been supported by the grants ANR-08-BLAN-0113-01 “PIWO”, ANR-2011-BS04-006-01 “ONLITUR” and CIBLE 2010 from Région Rhône-Alpes.

REFERENCES

[1] J. Lighthill, “Waves In Fluids”, (Cambridge University Press, London, 1978).
[2] J. Pedlosky, “Geophysical Fluid Dynamics”, (Springer-Verlag, Heidelberg, 1987).
[3] A. Fincham, G. Delerce, “Advanced optimization of correlation imaging velocimetry algorithms”, Experiments in Fluids **29**, 13 (2000).
[4] B.R. Sutherland, S.B. Dalziel, G.O. Hughes, and P.F. Linden, “Visualization and measurement of internal waves by synthetic schlieren. part 1. vertically oscillating cylinder”, Journal of Fluid Mechanics **390**, 93–126, (1999).
[5] L. Gostiaux, H. Didelle, S. Mercier, and T. Dauxois, “A novel internal waves generator”, Experiments in Fluids **42**, 123–130 (2007).
[6] M. Mercier, D. Martinand, M. Mathur, L. Gostiaux, T. Peacock, and T. Dauxois, “New wave generation”, Journal of Fluid Mechanics **657**, 308–1334 (2010).
[7] B.R. Sutherland, “Internal Gravity Waves”, (Cambridge University Press, London, 2010).

[8]M. Mathur, T. Peacock, “Internal wave interferometry”, Physical Review Letters **104**, 118501 (2010).

[9]T. Peacock, M.J. Mercier, H. Didelle, S. Viboud, and T. Dauxois, “A laboratory study of low-mode internal tide scattering by finite-amplitude topography”, Physics of Fluids **21**, 121702 (2009).

[10]S. Joubaud, J. Munroe, P. Odier, and T. Dauxois, "Experimental parametric subharmonic Instability in stratified fluids," submitted (2011).

[11]G. K. Vallis, “Atmospheric and Oceanic Fluid Dynamics”, (Cambridge University Press, London, 2006).

[12]T. Dauxois, W. R. Young, “Near critical reflection of internal waves”, Journal of Fluid Mechanics **390**, 271-295 (1999).

[13]A. Tabaei, T. R. Akylas, “Nonlinear internal gravity wave beams”, Journal of Fluid Mechanics **482**, 141-161 (2003).

[14]A. Tabaei, T. R. Akylas, K. G. Lamb, “Nonlinear effects in reflecting and colliding internal wave beams”, Journal of Fluid Mechanics **526**, 217-243 (2005).

[15]B. King, H.P. Zhang, H.L. Swinney, “Tidal flow over three-dimensional topography in a stratified fluid”, Physics of Fluids **21**, 116601 (2009).

[16]F. P. Bretherton, “On the mean motion induced by internal gravity waves”, Journal of Fluid Mechanics **36**, 785–803 (1969).

[17]M.-P. Lelong, J. Riley, “Internal wave-vortical mode interactions in strongly stratified flows”, Journal of Fluid Mechanics **232**, 1–19 (1991).

[18]J. Sommeria, LEGI / CNRS-UJF-INPG, `http://coriolis.legi.grenoble-inp.fr`.

[19]M. Mercier, N. Garnier, T. Dauxois, “Reflection and diffraction of internal waves analyzed with the Hilbert transform”, Physics of Fluids **20**, 0866015 (2008).

[20]M. Leclair, N. Grisouard, L. Gostiaux, C. Staquet, F. Auclair, “Reflexion of a plane wave onto a slope and wave-induced mean flow”, Stratified Flows conference, Roma (2011).

[21]L. Gostiaux, T. Dauxois, “Laboratory experiments on the generation of internal tidal beams over steep slopes”, Physics of Fluids **19**, 028102 (2007).